CHAPTER IV
RESULTS AND DISCUSSION

4.1 Catalyst Characterization

4.1.1 Elemental Analyses by XRF

Table 4.1 shows the chemical compositions obtained from XRF analyses, expressed as weight percentages, of the investigated catalysts. The fixed Ni content was at 15 wt% whereas Mg content was varied in the range of 1-3wt% of the catalyst. The composition of all elements was consistent with the theoretical value except that of Mg. It was found that Mg could be incorporated into $Ce_{0.75}Zr_{0.25}O_2$ lattices less than the desired values in which only ca. 13-15 wt% of added Mg could substitute into the ceria-zirconia mixed oxide structure. Actually, it was expected that the Mg should have incorporated more into the ceria lattice due to its small ionic radius (Ce^{4+}= 0.101 nm, Mg^{2+}= 0.072 nm) and form the solid-solution as suggested by Li and co-workers (2009). The reason for the less incorporation of Mg into ceria-zirconia lattice was probably that urea (sol-gel agent) was not suitable as a pH-adjusting agent in this system resulting in the formation of different Mg species which might be inappropriate for solid solution formation.

Table 4.1 Elemental analysis results for the catalysts synthesized

Catalyst	Composition (wt%)				
	Ce	Zr	Ni	Mg	O
$Ce_{0.75}Zr_{0.25}O_2$	65.61	14.37	-	-	20.02
$Ce_{0.75}Zr_{0.22}Mg_{0.07}O_2$	66.17	13.68	-	0.15	20.01
$Ce_{0.75}Zr_{0.15}Mg_{0.19}O_2$	66.43	13.16	-	0.38	20.04
$15Ni/Ce_{0.75}Zr_{0.25}O_2$	49.49	12.33	17.72	-	20.46
$15Ni/Ce_{0.75}Zr_{0.22}Mg_{0.07}O_2$	51.47	9.65	18.53	0.10	20.25
$15Ni/Ce_{0.75}Zr_{0.15}Mg_{0.19}O_2$	52.84	8.59	18.23	0.17	20.16

4.1.2 Textural Properties

Table 4.2 Textural properties of the investigated catalysts

Catalyst	BET surface area (m^2/g)	Pore volume (cm^3/g)	Average pore diameter* (nm)
$Ce_{0.75}Zr_{0.25}O_2$	84.56	0.07	4.27
$Ce_{0.75}Zr_{0.22}Mg_{0.07}O_2$	85.24	0.11	5.64
$Ce_{0.75}Zr_{0.15}Mg_{0.19}O_2$	81.95	0.10	5.24
$15Ni/Ce_{0.75}Zr_{0.25}O_2$	59.00	0.09	6.67
$15Ni/Ce_{0.75}Zr_{0.22}Mg_{0.07}O_2$	57.93	0.13	9.01
$15Ni/Ce_{0.75}Zr_{0.15}Mg_{0.19}O_2$	54.74	0.14	9.95

*obtained by BJH method

BET surface areas, pore volumes, and average pore diameters of the investigated catalysts are summarized in Table 4.2. The surface areas of all supports are ca.82-85 m^2/g with the average pore diameters of 4.3-5.6 nm. This is suggested that the incorporation of Mg into the ceria-zirconia lattices did not have an influence on the surface area of the resulted catalysts. When loading Ni onto these supports, it was found that the surface areas were reduced about 30-33 % due to the pore blockage of nickel species (Chen *et al.*, 2008).

4.1.3 X-ray Diffraction(XRD)

XRD patterns for all of the catalysts are shown in Figure 4.1. All the catalysts exhibited major peaks at ca. 28.8°, 33.5°, 47.5°, and 56.8° (2θ) representing the indices of (111), (200), (220) and (311) planes indicating a cubic fluorite structure of CeO_2 (Pengpanich *et al.*, 2002; Xu, S and Wang, X., 2005). Small peaks of NiO were observed at ca. 37.9°, 43.3°, and 62.7°(2θ) which is in good agreement with that reported by Bampenrat *et al.* (2010). No distinguishable peaks of MgO

could be observed for the catalysts prepared. This indicated the incorporation of Mg into the ceria-zirconia lattices and/or the small amount of Mg residing in the catalyst. The NiO particle sizes calculated from the Scherer's equation for the Ni-doped catalysts were ca. 27-30 nm.

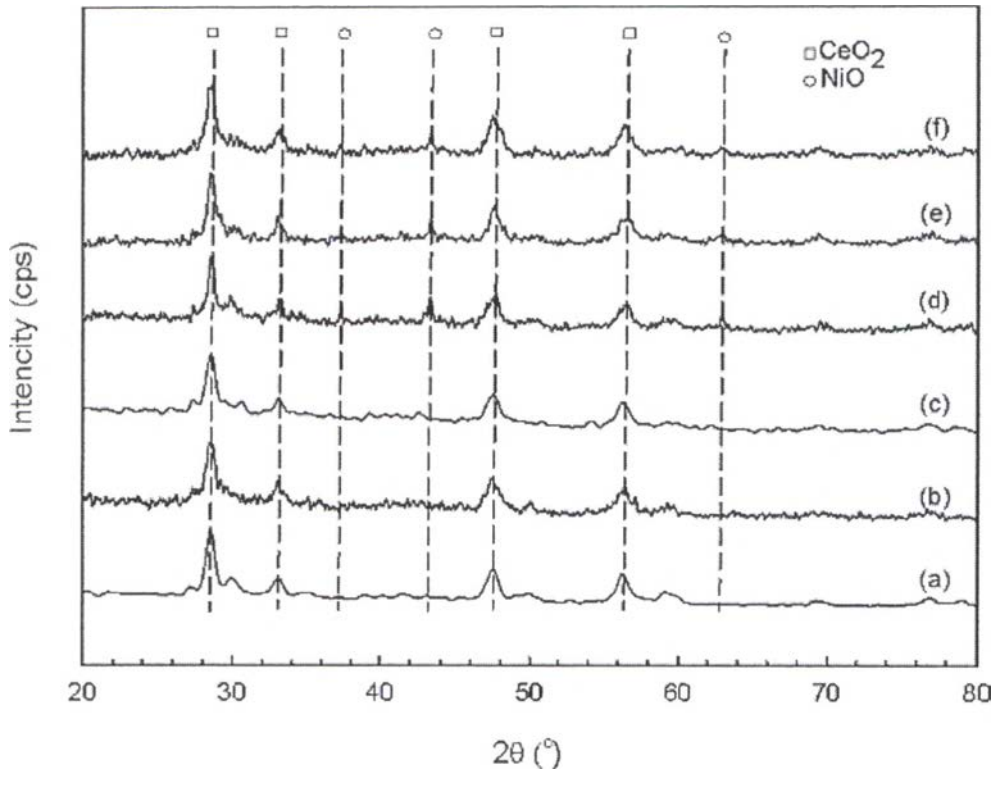

Figure 4.1 XRD patterns of the catalysts: (a) $Ce_{0.75}Zr_{0.25}O_2$, (b) $Ce_{0.75}Zr_{0.22}Mg_{0.07}O_2$, (c) $Ce_{0.75}Zr_{0.15}Mg_{0.19}O_2$, (d) $15Ni/Ce_{0.75}Zr_{0.25}O_2$, (e) $15Ni/Ce_{0.75}Zr_{0.22}Mg_{0.07}O_2$, (f) $15Ni/Ce_{0.75}Zr_{0.15}Mg_{0.19}O_2$.

4.1.4 TemperatureProgrammed Reduction by Hydrogen (H_2-TPR)

The reducibility of the catalysts evaluated by H_2-temperature programmed reduction (H_2-TPR) is shown in Figure 4.2. The TPR profiles of the supports possessed the small reduction peaks of surface and bulk CeO_2 at about 495-545°C and around 700-800°C. When Ni was loaded onto the supports, there were two additional peaks appearing as attributed to the free NiO species for the first peak and the complex NiO species for the second one. The comparisons of the TPR

profiles among the supports and the Ni-doped catalysts are illustrated in Figures 4.3 and 4.4, respectively.

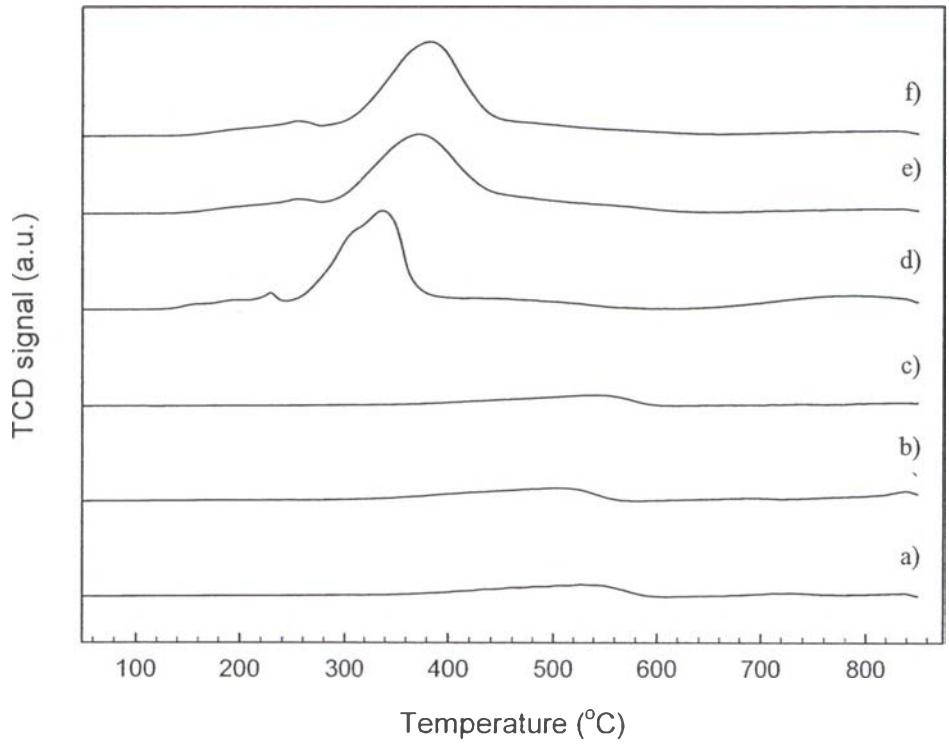

Figure 4.2 H_2-TPR profiles for the catalysts with a heating rate of 10 °C min^{-1}, a reducing gas containing 5% hydrogen in argon with a flow rate of 10 ml min^{-1}: a) $Ce_{0.75}Zr_{0.25}O_2$, b) $Ce_{0.75}Zr_{0.22}Mg_{0.07}O_2$,c) $Ce_{0.75}Zr_{0.15}Mg_{0.19}O_2$, d) $15Ni/Ce_{0.75}Zr_{0.25}O_2$, e) $15Ni/Ce_{0.75}Zr_{0.22}Mg_{0.07}O_2$, f) $15Ni/Ce_{0.75}Zr_{0.15}Mg_{0.19}O_2$.

Figure 4.3 shows the H_2-TPR profiles for the supports. The $Ce_{0.75}Zr_{0.25}O_2$ (CZO) possesses two reduction peaks, a main peak appearing at ca. 495°C and the other small one occurring at ca. 720 °C, corresponding to the reductions of surface oxygen and bulk oxygen, respectively (Pengpanich *et al.*, 2002). The $Ce_{0.75}Zr_{0.22}Mg_{0.07}O_2$ (CZM1O) exhibits two distinguishable reduction peaks at 495°C and ca. 700-800°C while the $Ce_{0.75}Zr_{0.15}Mg_{0.19}O_2$ (CZM3O) shows an only reduction peak at ca. 545°C. The results indicated that both the CZM1O and

CZO are more facile to be reduced than the CZM3O. This suggested the intervention of Mg species in ceria-zirconia lattices of the CZM3O.

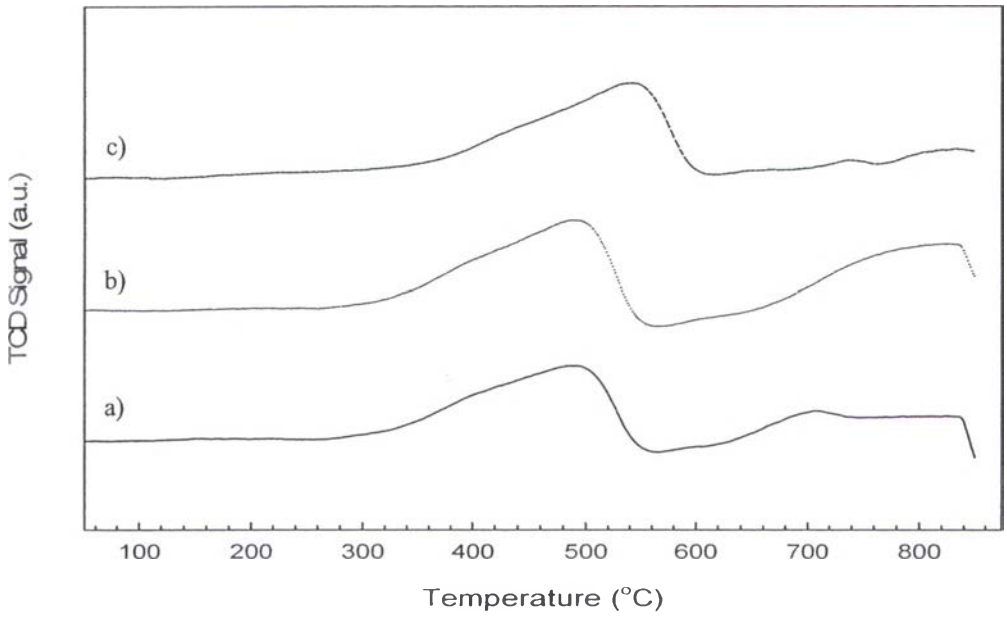

Figure 4.3 H_2-TPR profiles for the supports with a heating rate of 10 °C min^{-1}, a reducing gas containing 5% hydrogen in argon with a flow rate of 10 ml min^{-1}: a) $Ce_{0.75}Zr_{0.25}O_2$ (CZO), b) $Ce_{0.75}Zr_{0.22}Mg_{0.07}O_2$(CZM1O), and c) $Ce_{0.75}Zr_{0.15}Mg_{0.19}O_2$ (CZM3O)

The reducibility of Ni-doped catalysts is shown in Figure 4.4. The Ni/CZO catalyst possesses two reduction peaks at ca. 230 and 340°C, and a small broad peak at ca. 800 °C. The reduction peak at ca. 230 °C was ascribed to the free NiO species interacting weakly with support and the other peak at ca. 340 °C was attributed to the complex NiO species interacting strongly with support (Pengpanich *et al.*, 2004). The small broad reduction peak at 800 °C was contributed to the bulk reduction of CeO_2. Both the Ni/CZM1O and Ni/CZM3O catalysts exhibit similar reduction peaks at 260 and 370 °C which were assigned to the reductions of free NiO and complex NiO, respectively in the absence of the small broad reduction peak at ca. 800 °C. Besides, it was observed that the reduction peaks of both the free NiO and complex NiO species for the Mg-containing catalysts were smaller and broader than that of the Ni/CZO. It implies that the interactions of the impregnated NiO with

the MgO residing in ceria-zirconia support caused the decline in reducibility of NiO species in the Mg-containing catalysts.

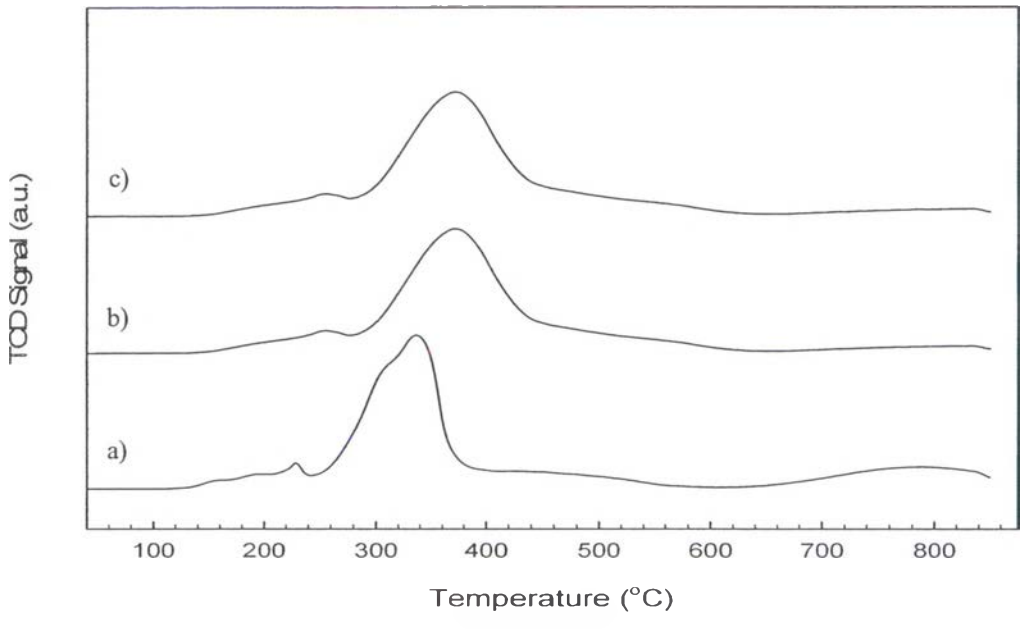

Figure 4.4 H_2-TPR profiles for the catalysts with a heating rate of 10 °C min^{-1}, a reducing gas containing 5% hydrogen in argon with a flow rate of 10 ml min^{-1}: a) $15Ni/Ce_{0.75}Zr_{0.25}O_2$ (Ni/CZO), b) $15Ni/Ce_{0.75}Zr_{0.22}Mg_{0.07}O_2$ (Ni/CZM1O), and c) $15Ni/Ce_{0.75}Zr_{0.15}Mg_{0.19}O_2$ (Ni/CZM3O).

4.1.5 Scanning Electron Microscopy (SEM)

Figure 4.5 shows SEM images of all the catalysts investigated. For the supports, both the modified and unmodified CZO present a similar morphology of the ceria-zirconia mixed oxide. All of which illustrate the aggregation of the primary long thin needle shaped particles [(a) to (c)] were similar to those observed by Thammachart and colleagues (2001). The morphology of the individual Ni-doped catalysts [(d) to (f)] was similar to one another depicting the round particles of the NiO particle attached onto the surface of supports.

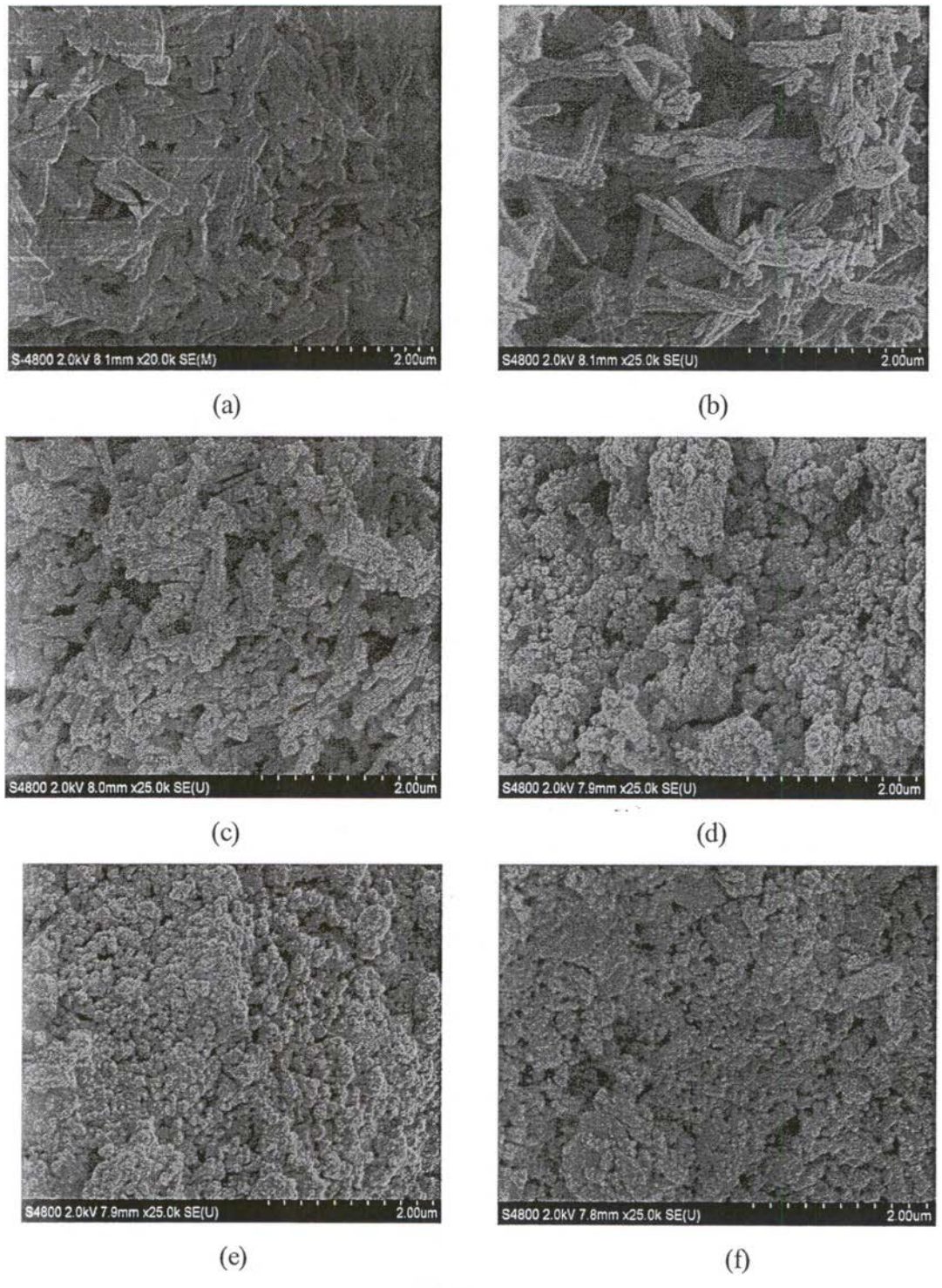

Figure 4.5 SEM images (20000x magnifications) of a) CZO b) CZM1O c) CZM3O d) NiO/CZO, e) NiO/CZM1O, f) NiO/CZM3O

4.2 Catalytic Activities for Catalytic Partial Oxidation of Methane

4.2.1 Catalytic Activities for CPOM

The evaluations on catalytic activities of all catalysts for CPOM were carried out under the following reaction conditions: CH_4/O_2 ratio of 2.0, GHSV of 53000 h^{-1}, and an atmospheric pressure. For the supports, it was observed that all the supports catalyzed only the total oxidation reaction providing only CO_2 and H_2O as products. This observation is in good agreement with that reported by Otsuka *et al.* (1999) who studied the reaction of CH_4 with CeO_2 in the presence of gaseous O_2. They found that the CO_2 and H_2O were the main products under such a condition. Both the CZO and CZM1O supports provided the comparable methane conversion whereas the CZM3O gave slightly higher methane conversion and CO_2 yield than the others. However, the methane conversion of these supports was less than 21% at the highest temperature.

When Ni was doped onto these supports, it was found that these catalysts showed the CPOM activity at temperatures higher than 500°C and 550°C for the Ni/CZO and Ni/CZMxO (x=1 and 3) catalysts, respectively. The highest methane conversion was achieved at ca. 85% for all the Ni-doped catalysts studied. Moreover, at temperatures less than the temperature that actives to CPOM, the Ni-doped catalysts provided much better CO_2 yield than the corresponding supports. Also, after the CPOM activated temperature was reached, the CO_2 yield was dropped rapidly while the syngas (H_2 and CO) yield was dramatically increased at this initial temperature. All of the Ni-doped catalysts behaved in similar manners for catalytic activity in CPOM and selectivity to CPOM products.

Although the supports showed similar trends in activity and selectivity to the combustion reaction, they showed the differences in O_2 consumption and CO_2 yield. As illustrated in Figure 4.6, it was noticed that the CZM3O support exhibited the highest O_2 consumption at all the temperatures investigated. This implied the increases in oxygen diffusion and oxygen mobility resulting from the incorporation of a proper amount of Mg into the ceria-zirconia lattices. However, there were no significant changes in O_2 conversion between the CZO and CZM1O supports. This is probably due to the infinitesimal amount of Mg content incorporated into the ceria-zirconia structure of CZM1O. The CO_2 yields of the supports are shown in Figure 4.7. For the supports, the CO_2 yield was increased with increasing temperature and reached its maximum value at

750°C where the oxygen was completely consumed. The methane conversions of all supports were achieved their maxima at 750°C with only ca. 21% conversion as illustrated in Figure 4.8. It can be explained that the conversion of methane was limited by the less amount of oxygen fed at this reaction temperature. Among the supports, the CZM3O exhibited the best performance in combustion reaction due to the improvement of oxygen mobility in the ceria-zirconia structure after the incorporation of a proper amount of Mg.

When the supports were doped with Ni, they showed the slightly increased methane conversion and substantially increased oxygen consumption. This is because NiO species acted as a catalyst catalyzing the combustion reaction. After the CPOM activated temperatures were achieved, both CO_2 and methane were drastically consumed as shown in Figures 4.7 and 4.8. This might be due to the fact that, at such temperatures, the reforming reactions in turn took place in which the remaining methane was consecutively reacted with the combustion products resulting in the syngas formation as evidenced in Figures 4.9 and 4.10.

For the Ni-doped catalysts, the Ni/CZO initially started the CPOM reaction at 500 °C while those Mg-containing catalysts started at a higher temperature of 550°C. This indicates that the addition of Mg retarded the activation energy for CPOM. This can be explained that the doped-NiO species formed the strong interactions with the CZMO support evident by the increase in reduction temperature of the complex NiO species as discussed in H_2-TPR analysis (Figure 4.4). This observation is in good agreement with that proposed by Arunsingkarat *et al.* (2012).

Amongst the Ni-doped catalysts, the Ni/CZM3O exhibited the highest methane conversion, H_2 and CO yields while those of the Ni/CZO and Ni/CZM1O were comparable. This is probably due to the enhancement of O_2 mobility promoted by the proper amount of Mg incorporated into the ceria-zirconia lattices. Since the more CO_2 was produced, the more reactant to react with the remaining methane via dry reforming reaction was. This would benefit the syngas yield and increase in methane conversion. Moreover, it was suggested by Zanganeh *et al.* (2013) that the basicity of MgO caused the strong adsorption for CO_2. This could also be a reason for the explanation on the enhanced catalytic activity of the Ni/CZM3O catalyst.

For Ni/CZO and Ni/CZM1O, both showed similar methane conversion, H_2 and CO yields at the temperatures investigated. This is due to the amount of Mg

incorporated in ceria-zirconia mixed oxide was insufficient to promote the O_2 mobility of the resulting catalyst resulting in the insignificant changes in CPOM performance.

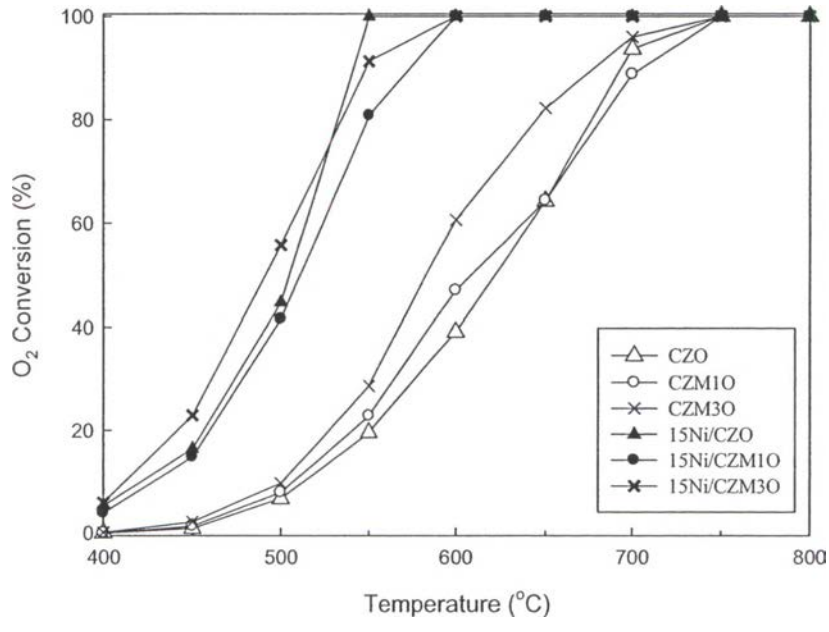

Figure 4.6 O_2 conversions at different temperatures over the investigated catalysts using CH_4/O_2 ratio = 2:1 and GHSV = 53000 h^{-1}.

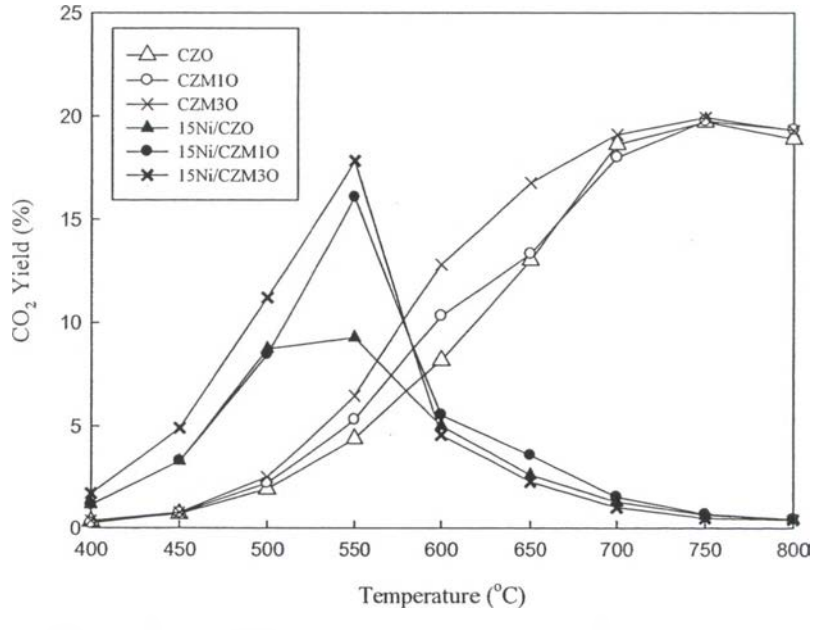

Figure 4.7 CO_2 yields at different temperatures over the investigated catalysts using CH_4/O_2 ratio = 2:1 and GHSV = 53000 h^{-1}.

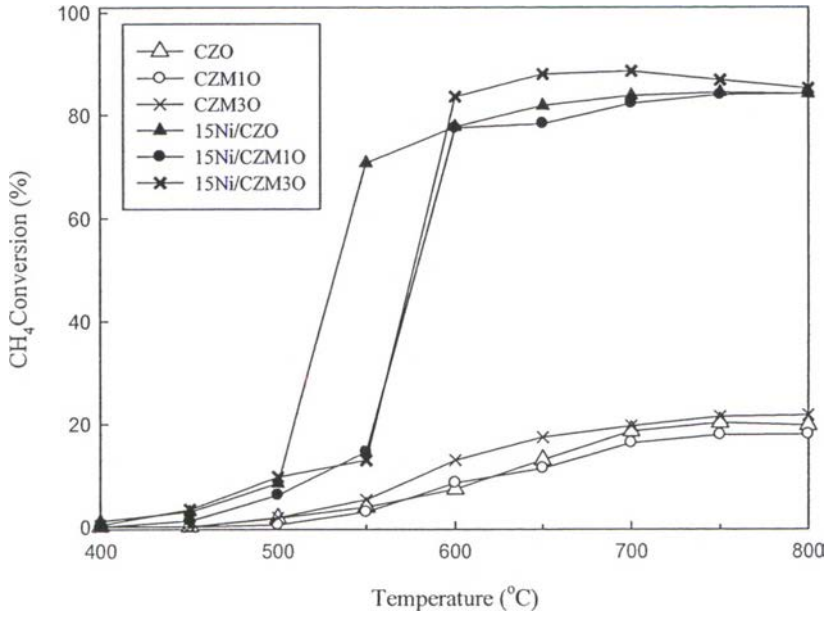

Figure 4.8 Methane conversions at different temperatures over the investigated catalysts using CH_4/O_2 ratio = 2:1 and GHSV = 53000 h^{-1}.

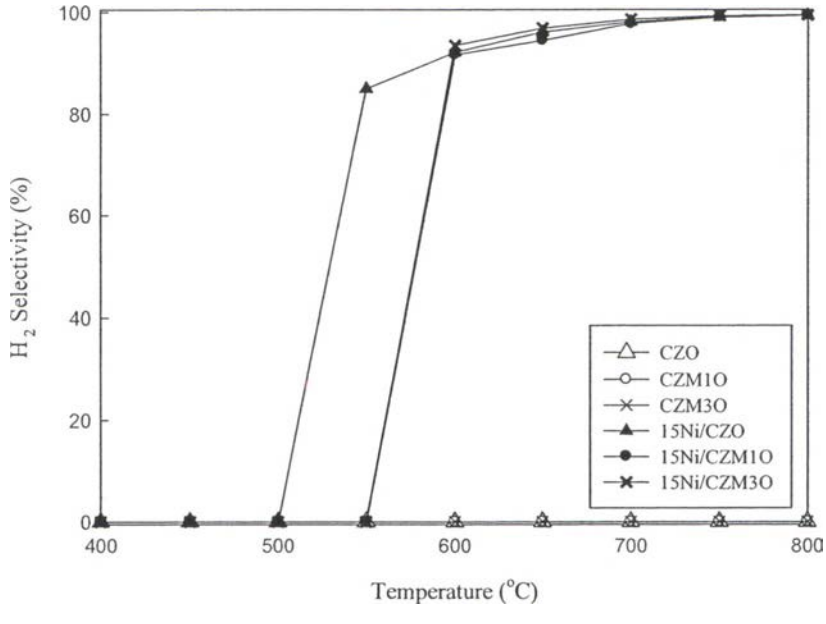

Figure 4.9 H_2 selectivities at different temperatures over the investigated catalysts using the CH_4/O_2 ratio = 2:1 and GHSV = 53000 h^{-1}.

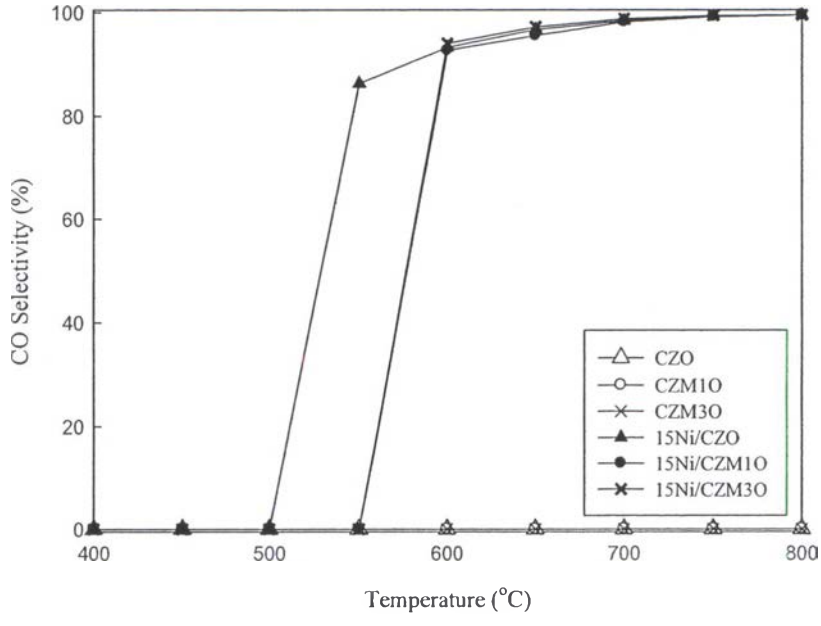

Figure 4.10 CO selectivities at different temperatures over the investigated catalysts using the CH_4/O_2 ratio = 2:1 and GHSV = 53000 h^{-1}.

Figures 4.7 and 4.11 show the CO_2 yield and CO_2 selectivity, respectively. As mentioned above, the main products of the supports were the combustion products. For the Ni-doped catalysts, after the CPOM temperature was reached, the selectivity and yield of synthesis gas were rapidly increased (Figs. 4.9, 4.10, 4.12, and 4.13) whereas those of combustion products were drastically decreased (Figs. 4.7 and 4.11). The results suggest that the synthesis gas occurred via the combustion and reforming reaction mechanism (CRR mechanism). The combustion reaction occurred first giving CO_2 and H_2O as the primary products, and then, the unreacted methane would react with the CO_2 and H_2O via dry and steam reforming reactions, respectively, providing CO and H_2 as the secondary products (Tsipouriari *et al.*, 1997; York *et al.*, 2011). This observation is similar to that observed by Pengpanich *et al.* (2004) who studied the CPOM over the $Ni/Ce_{1-x}Zr_xO_2$ (x=0, 0.25 and 1.0) catalysts. They reported the observation of the CO_2 and H_2O as the main products at temperature below 550°C.

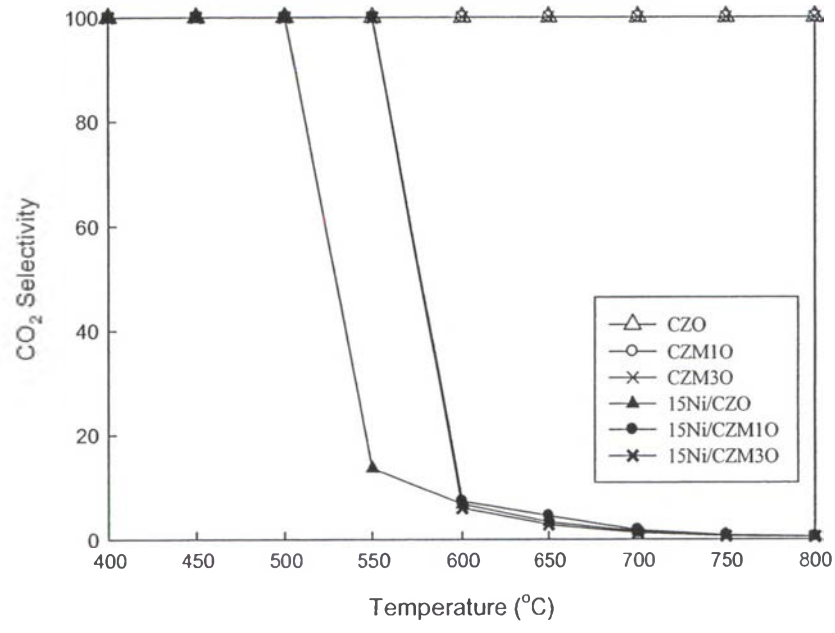

Figure 4.11 CO_2 selectivities at different temperatures over the investigated catalysts using the CH_4/O_2 ratio = 2:1 and GHSV = 53000 h^{-1}.

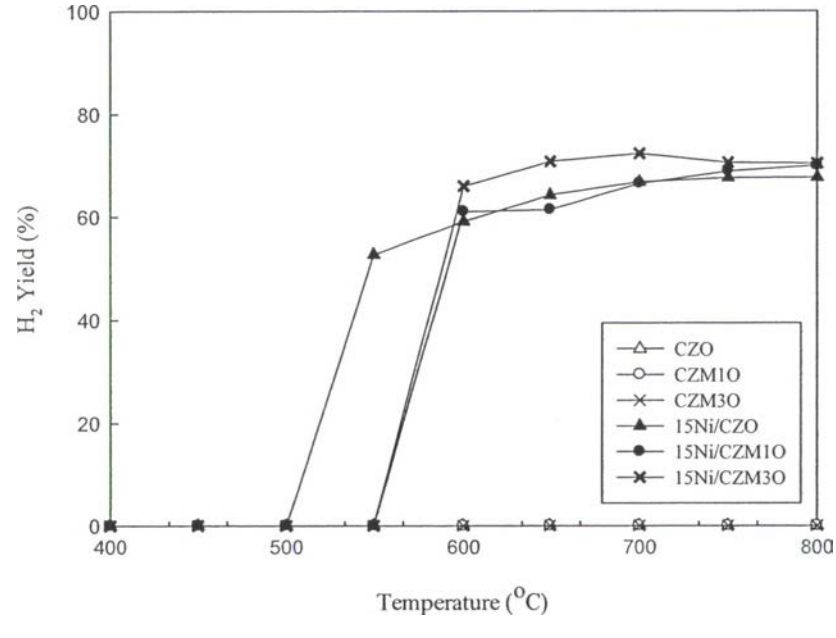

Figure 4.12 H_2 yields at different temperatures over the investigated catalysts using CH_4/O_2 ratio = 2:1 and GHSV = 53000 h^{-1}.

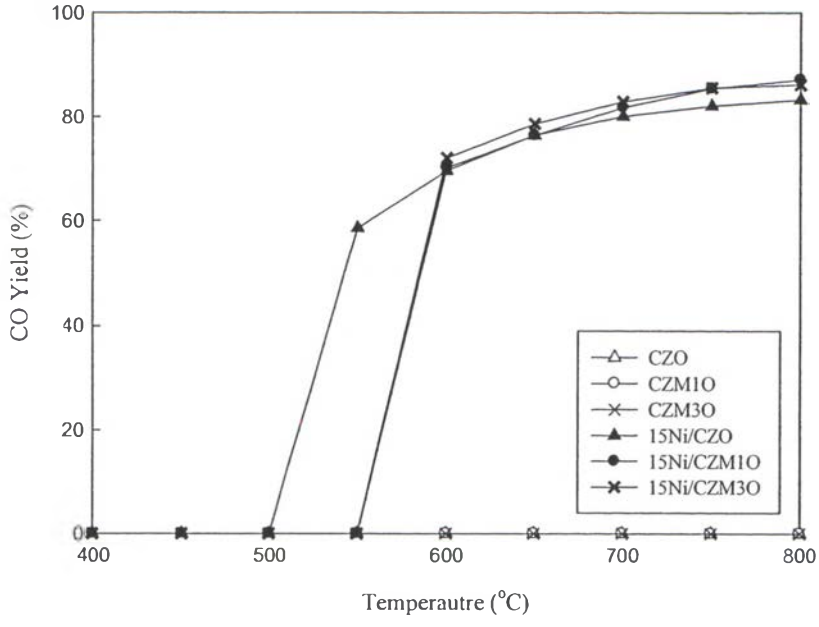

Figure 4.13 CO yields at different temperatures over the investigated catalysts using CH_4/O_2 ratio = 2:1 and GHSV = 53000 h^{-1}.

The H_2/CO ratios of the investigated catalysts at various temperatures are presented in Figure 4.14. The H_2/CO ratio of the Ni-doped catalysts was initially about 1.9 and continued to decrease with increasing the reaction temperature. This can be explained that there was the reverse water gas shift reaction ($CO_2+H_2 \rightarrow CO+H_2O$; ΔH=41.1 kJ/mol) occurring during the course of reactions resulting in the gradual decrease in H_2/CO ratio to be below the theoretical value of 2.

4.2.2 Catalyst Stability for CPOM

The catalytic stability tests were performed on the Ni-doped catalysts under the following reaction conditions: 750°C, CH_4/O_2 ratio of 2.0, GHSV of 53000 h^{-1} and an atmospheric pressure.

Figures 4.15-4.20 illustrate the methane conversions, hydrogen and carbon monoxide selectivities and yields, carbon dioxide yields and H_2/CO ratios for the investigated catalysts, respectively.

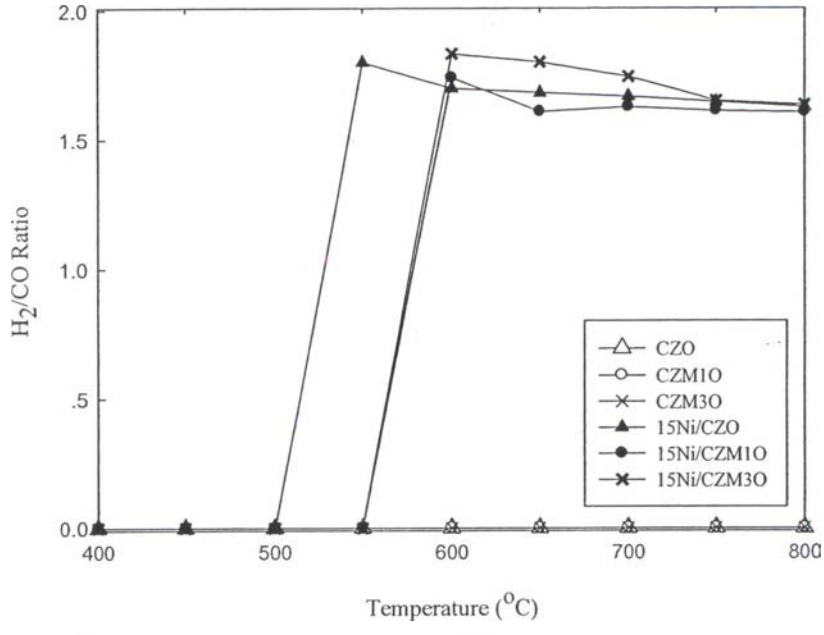

Figure 4.14 H_2/CO ratios at different temperatures over the investigated catalysts using CH_4/O_2 ratio = 2:1 and GHSV = 53000 h^{-1}.

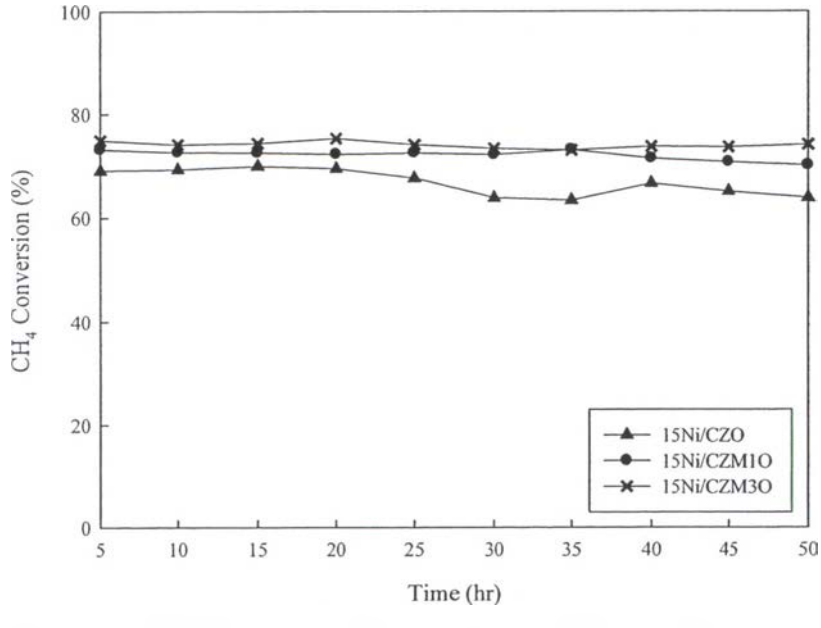

Figure 4.15 CH_4 conversion as a function of time over the catalysts investigated at 750°C (CH_4/O_2 ratio of 2:1, GHSV = 53000 h^{-1}).

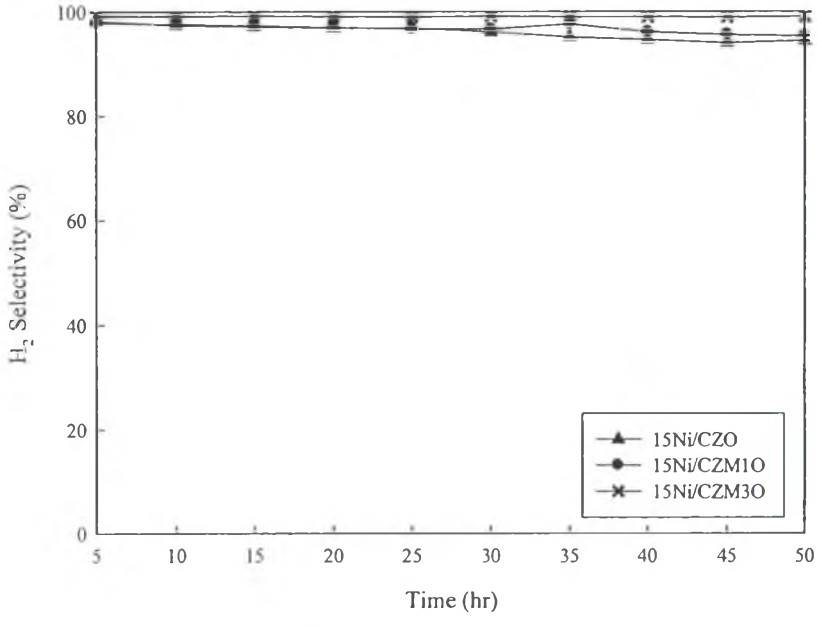

Figure 4.16 H_2 selectivities as a function of time over the catalysts investigated at 750°C (CH_4/O_2 ratio of 2:1, GHSV = 53000 h^{-1}).

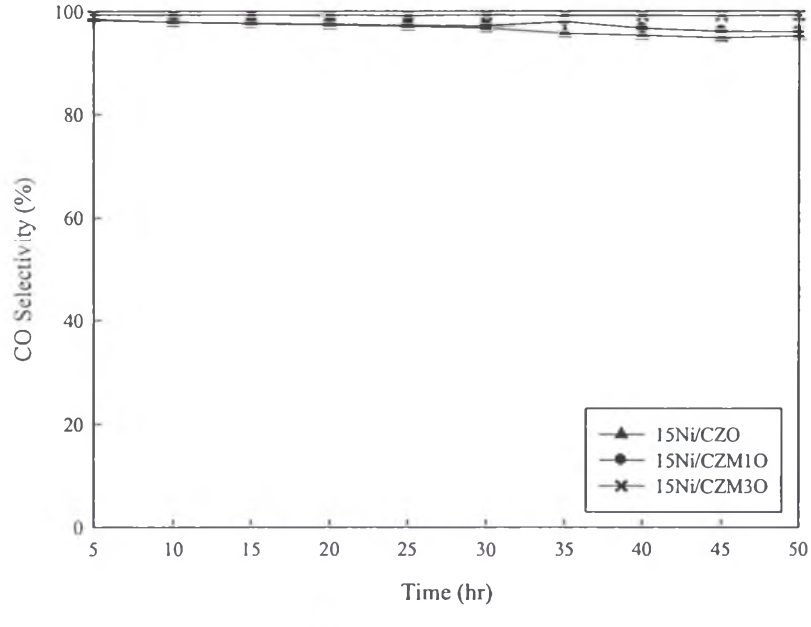

Figure 4.17 CO selectivities as a function of time over the catalysts investigated at 750°C (CH_4/O_2 ratio of 2:1, GHSV = 53000 h^{-1}).

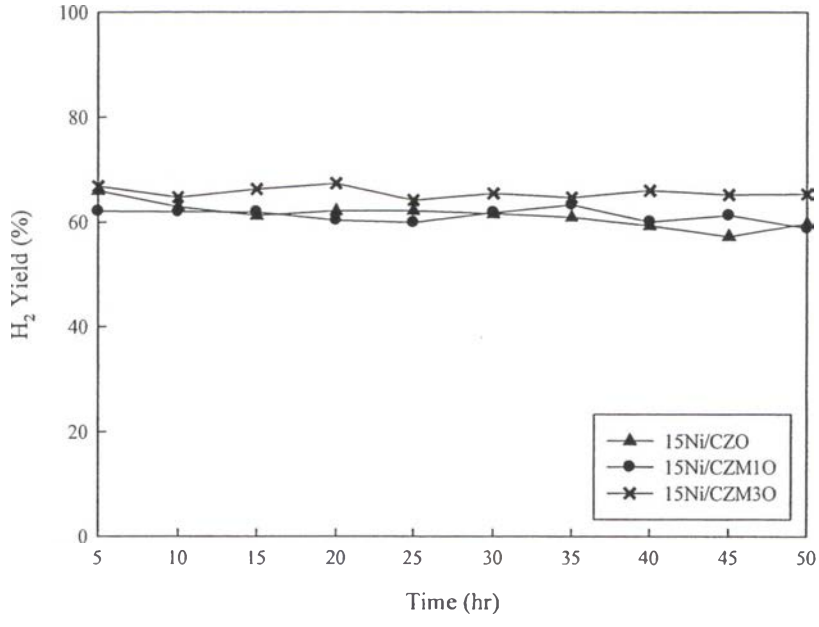

Figure 4.18 H_2 yields as a function of time over the catalysts investigated at 750°C (CH_4/O_2 ratio of 2:1, GHSV = 53000 h^{-1}).

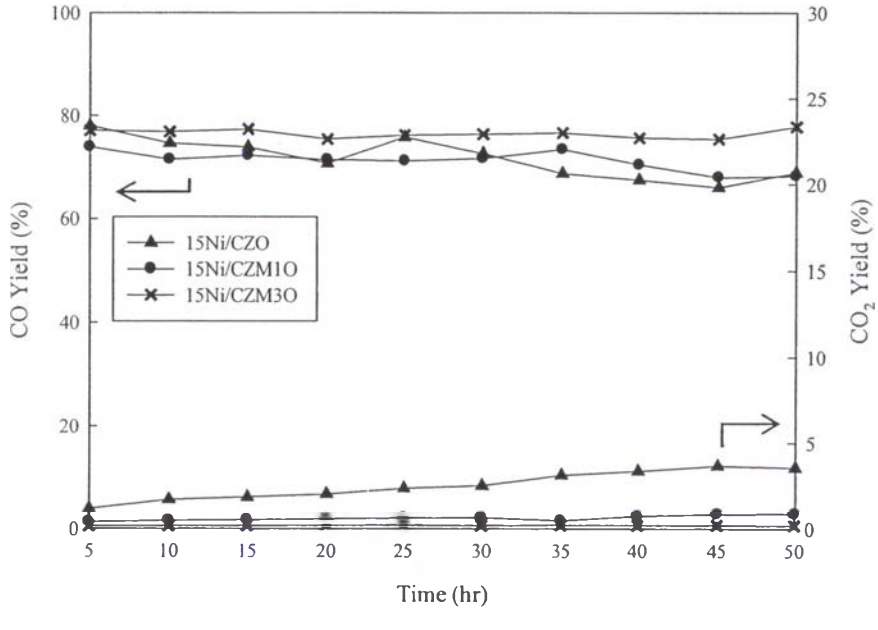

Figure 4.19 CO yields as a function of time over the catalysts investigated at 750°C (CH_4/O_2 ratio of 2:1, GHSV = 53000 h^{-1}).

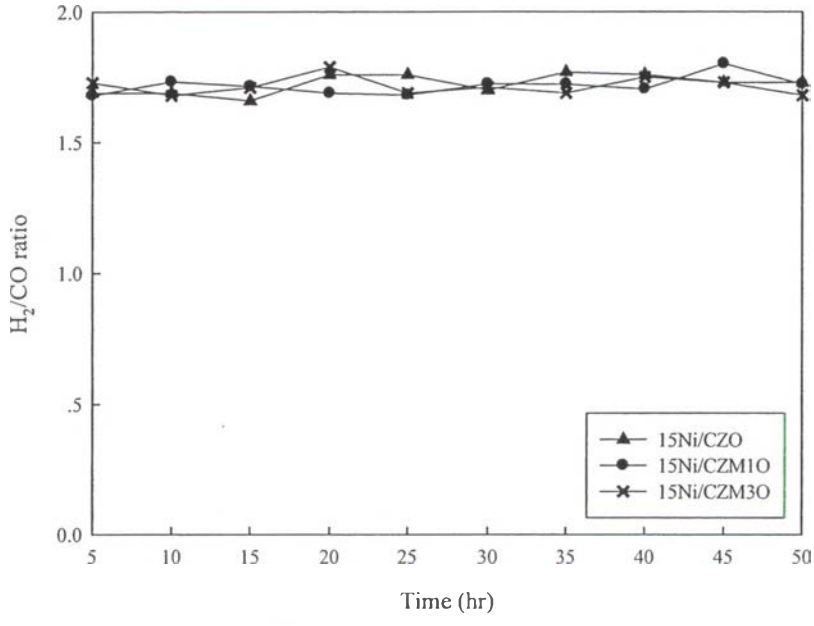

Figure 4.20 H_2/CO ratios as a function of time over the catalysts investigated at 750°C (CH_4/O_2 ratio of 2:1, GHSV = 53000 h^{-1}).

Both the Ni/CZM1O and Ni/CZM3O showed insignificant decreases in CH_4 conversion, H_2 and CO selectivity and yield whereas the Ni/CZO exhibited slight decreases in those with time on stream (TOS). This indicates that the incorporation of Mg improved the stability of Ni/CZO catalyst resulting from the strong interactions between the NiO species and CZMO support to prohibit the agglomeration of NiO particles. Figure 4.19 illustrates the CO_2 yields as a function of time of the investigated catalysts, the CO_2 yield of Ni/CZO was increased with TOS while those of Ni/CZM1O and Ni/CZM3O were invariably changed. This indicates that the incorporation of Mg into ceria-zirconia lattice helped prevent the catalytic deactivation of Ni/CZO. Moreover, it is known that a proper amount of MgO loading can improve dispersion and basicity of the resulted catalyst. (Yejun *et al.*, 2007) This would bring about the improvement of catalyst stability due to the reduction of carbon deposition on the catalyst surface. The H_2/CO ratios of all investigated catalysts were insignificant changed with TOS indicating that no intervention from the reverse water gas shift reaction occurring at temperature of 750°C for all investigated catalysts.

The investigation on catalytic activity of the Ni-doped catalysts after regeneration under 10% O_2 balanced with He at 750°C for 10 h was conducted and their results are shown in Figures 4.21-4.29. The Ni/CZO catalyst possessed the decreased H_2 and CO yields and the increased CO_2 yield indicating the deterioration in the reforming activity as presented in Figures 4.21-4.23. The original catalytic activity and products yield for both the Ni/CZM1O and Ni/CZM3O catalysts were regained as shown in Figures 4.24-4.29. The deactivation of Ni/CZO in the second evaluation was resulted from the filamentous carbon formation causing the disintegration of nickel particles to be in the unsuitable form to catalyze the reforming reaction after regeneration as shown in Figure 4.30. This phenomenon was reasonable to explain the insignificant change in methane conversion but the drastic drop in synthesis gas yield for the Ni/CZO in the second evaluation. The incorporation of Mg into ceria-zirconia lattices enhanced the attachment of nickel particle with the support by metal-support interaction which could reduce the destruction of nickel particles caused by filamentous carbon formation resulting in the better stability of the Ni/CZM1O and Ni/CZM3O catalysts.

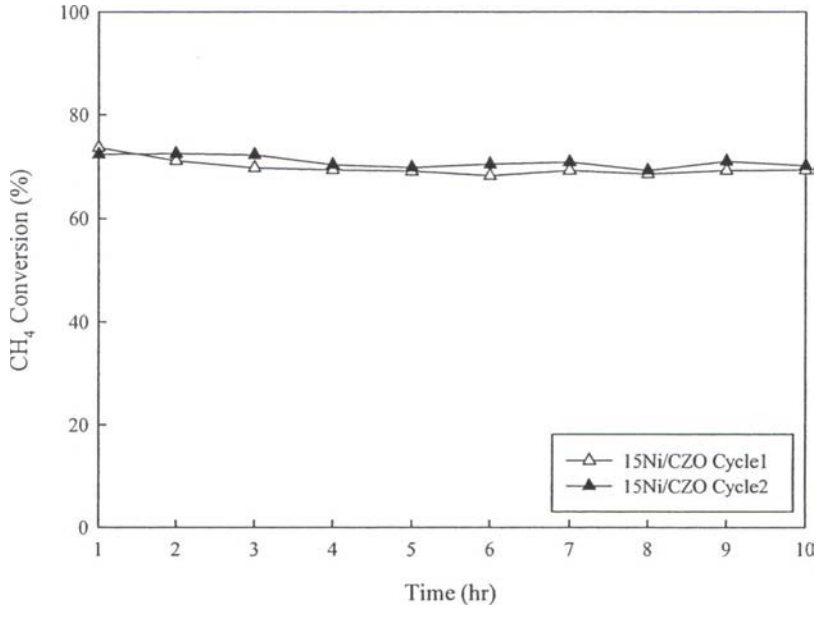

Figure 4.21 CH_4 conversions as a function of time over the Ni/CZO catalyst at temperature of 750°C (CH_4/O_2 ratio of 2.0, GHSV = 53000 h^{-1}) compared with the regenerated catalysts with 10% O_2 in He, at 750°C, for 2 h.

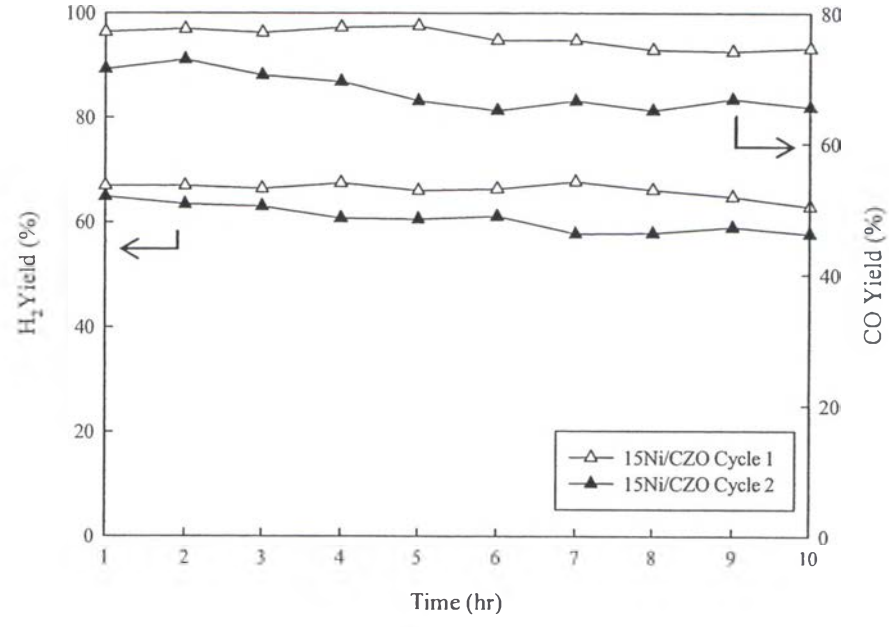

Figure 4.22 H_2 and CO yields as a function of time over the Ni/CZO catalyst at temperature of 750°C (CH_4/O_2 ratio of 2.0, GHSV = 53000 h^{-1}) compared with the regenerated catalysts with 10% O_2 in He, at 750°C, for 2 h.

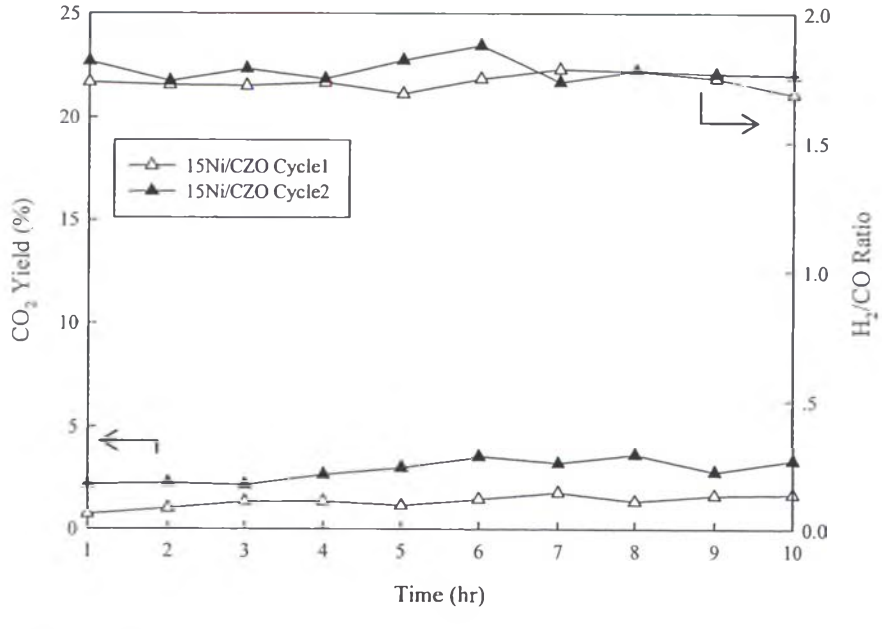

Figure 4.23 CO_2 yields and H_2/CO ratios as a function of time over the Ni/CZO catalyst at temperature of 750°C (CH_4/O_2 ratio of 2.0, GHSV = 53000 h^{-1}) compared with the regenerated catalysts with 10% O_2 in He, at 750°C, for 2 h.

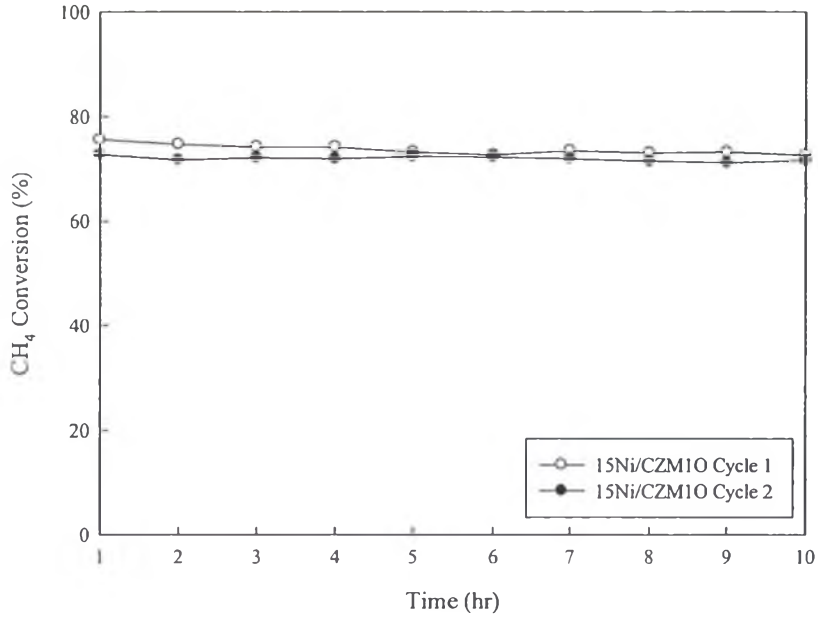

Figure 4.24 CH_4 conversions as a function of time over the Ni/CZM1O catalyst at temperature of 750°C (CH_4/O_2 ratio of 2.0, GHSV = 53000 h^{-1}) compared with the regenerated catalysts with 10% O_2 in He, at 750°C, for 2 h.

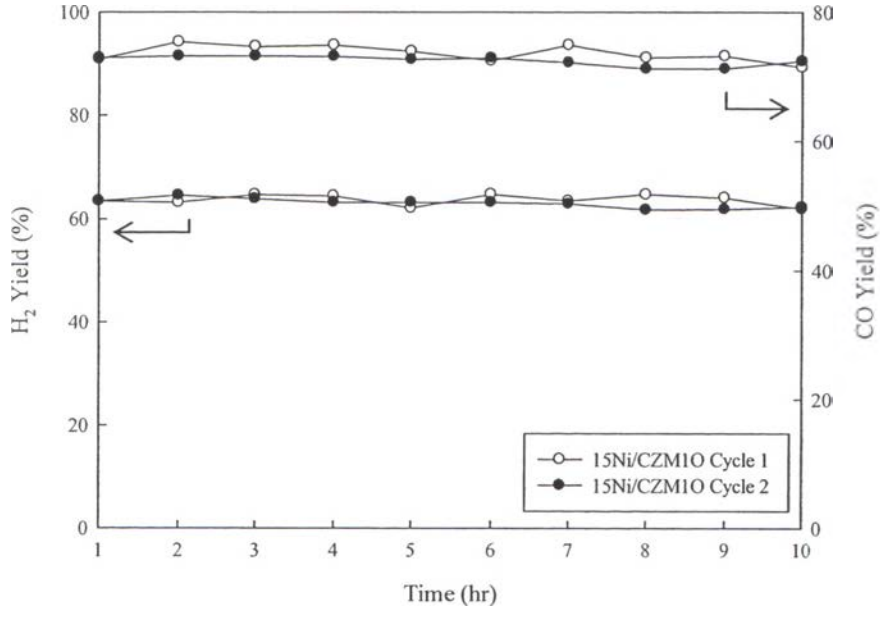

Figure 4.25 H_2 and CO yields as a function of time over the Ni/CZM1O catalyst at temperature of 750°C (CH_4/O_2 ratio of 2.0, GHSV = 53000 h^{-1}) compared with the regenerated catalysts with 10% O_2 in He, at 750°C, for 2 h.

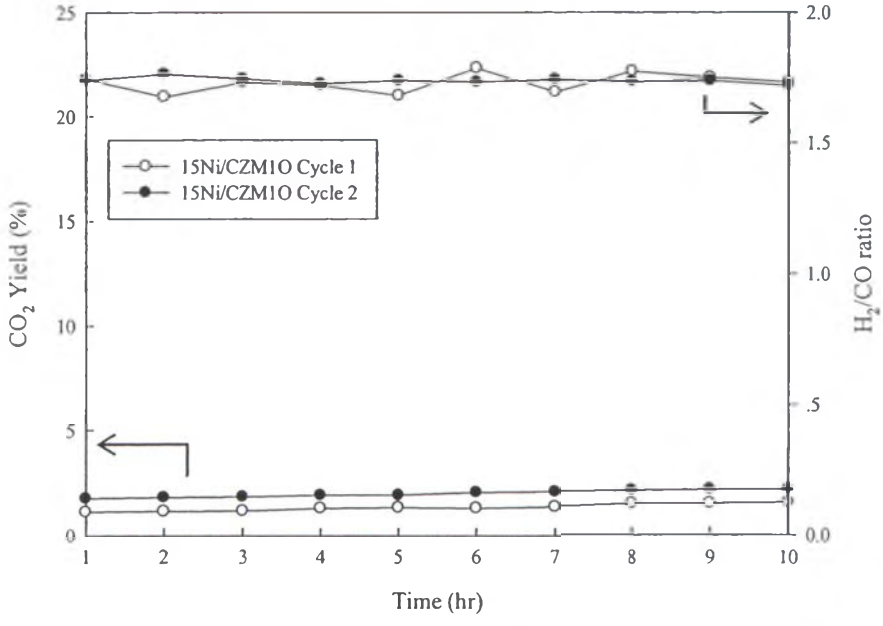

Figure 4.26 CO_2 yields and H_2/CO ratios as a function of time over the Ni/CZM1O catalyst at temperature of 750°C (CH_4/O_2 ratio of 2.0, GHSV = 53000 h^{-1}) compared with the regenerated catalysts with 10% O_2 in He, at 750°C, for 2 h.

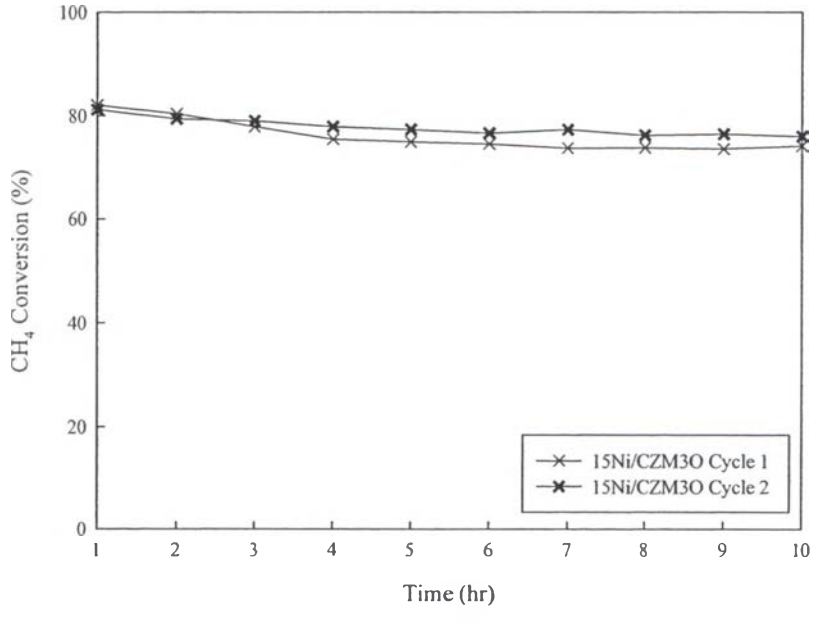

Figure 4.27 CH_4 conversions as a function of time over the Ni/CZM3O catalyst at temperature of 750°C (CH_4/O_2 ratio of 2.0, GHSV = 53000 h^{-1}) compared with the regenerated catalysts with 10% O_2 in He, at 750°C, for 2 h.

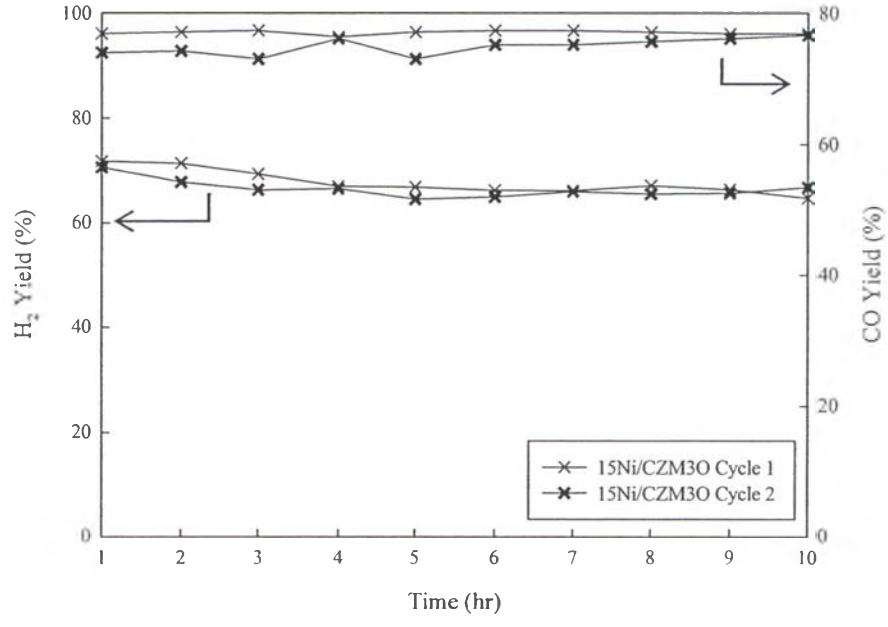

Figure 4.28 H_2 and CO yields as a function of time over the Ni/CZM3O catalyst at temperature of 750°C (CH_4/O_2 ratio of 2.0, GHSV = 53000 h^{-1}) compared with the regenerated catalysts with 10% O_2 in He, at 750°C, for 2 h.

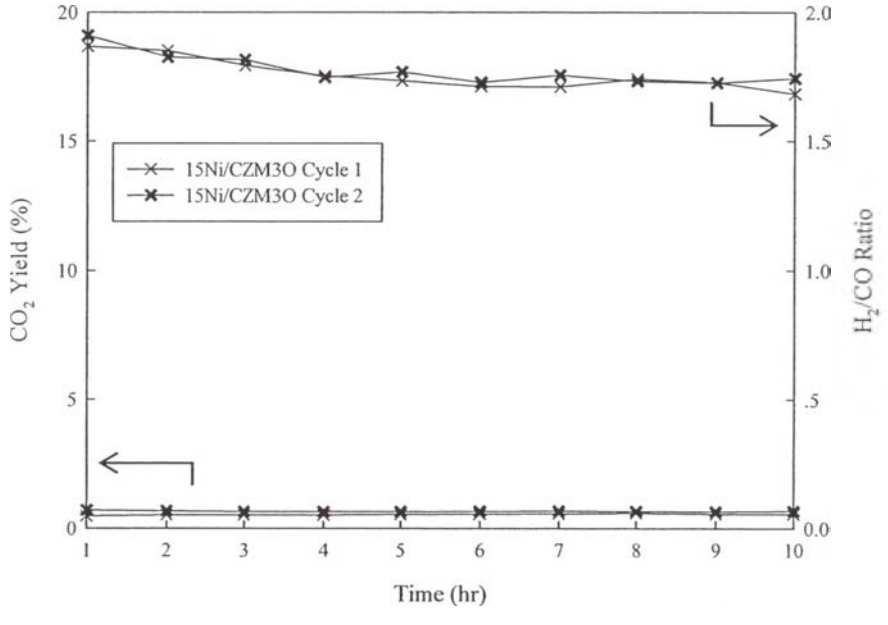

Figure 4.29 CO_2 yields and H_2/CO ratios as a function of time over the Ni/CZM3O catalyst at temperature of 750°C (CH_4/O_2 ratio of 2.0, GHSV = 53000 h^{-1}) compared with the regenerated catalysts with 10% O_2 in He, at 750°C, for 2 h.

Figure 4.30 shows the TEM images of the spent Ni-doped catalysts after the second evaluation on catalytic performance. The filamentous carbon growth was observed for all the spent Ni-doped catalysts. It is interesting to note that the spent Ni/CZO catalyst possessed the filament growth from some detached nickel particles being at the middle and at the tip of the filamentous carbon whereas both the Ni/CZM1O and Ni/CZM3O catalysts exhibited the filament growth from the surface of nickel particles attached onto the support.. It is obviously visualized that the Ni/particles strongly attached onto the CZMO support due to the strong metal-support interaction. The results are in agreement with those obtained from the activity tests and from the second evaluation on catalytic performance after regeneration which indicated that the Ni/CZO catalyst showed the lost in catalytic activity whereas the Ni/CZMO catalysts showed the stability in catalytic performance over the period of time on stream for both before and after regeneration.

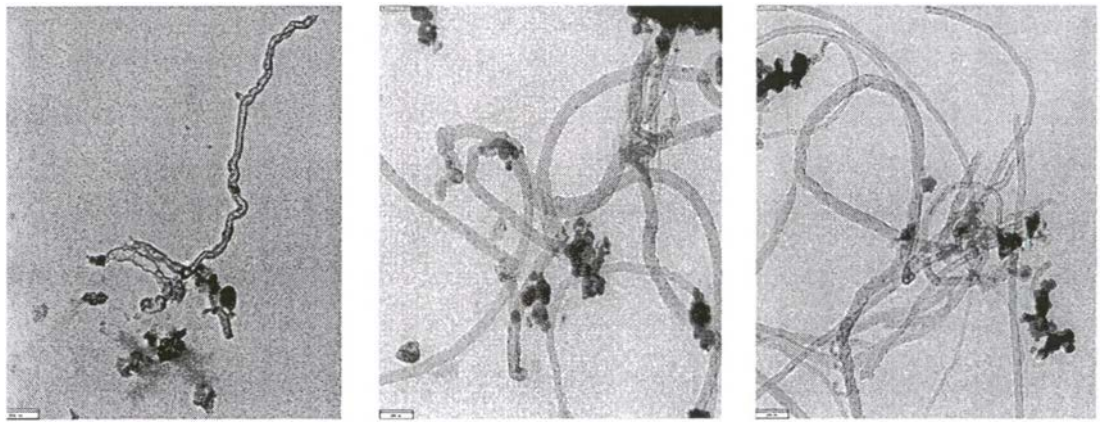

a) b) c)

Figure 4.30 TEM images of the spent catalysts after the second evaluation on the catalytic performance at 750°C (CH_4/O_2 = 2.0, GHSV = 53,000 h^{-1}) for 10 hours: a) Ni/CZO, b) Ni/CZM1O and c) Ni/CM3O

Figure 4.31 presents SEM images of the spent catalysts after performing the CPOM reaction. As compared with fresh catalysts shown in Figure 4.5, it is observed that the spent CZO and CZMxO (x=1 and 3) supports exhibited larger size than the fresh supports. This is because the agglomeration of the support particles subjected to a high reaction temperature. Besides, there is the absence of

carbon as observed by SEM on the surfaces of CZO and CZMO supports. This is implied that the coke formation would come from the dissociation of CH_4 and/or the reaction of CO through methane decomposition and Boudouard reaction consecutively which occurred on the surface of Ni metal particles. For the spent Ni-doped catalysts, the filamentous carbon formed is clearly seen by SEM. The results are conformed to the TPO results of the spent Ni-doped catalysts (Appendix E) and the TEM images of the spent Ni-doped catalysts. It is suggested that the carbon formation on the Ni/CZO catalyst was mainly derived from the methane decomposition reaction which is favorable at high reaction temperatures (Pengpanich *et al.*, 2004).

a)

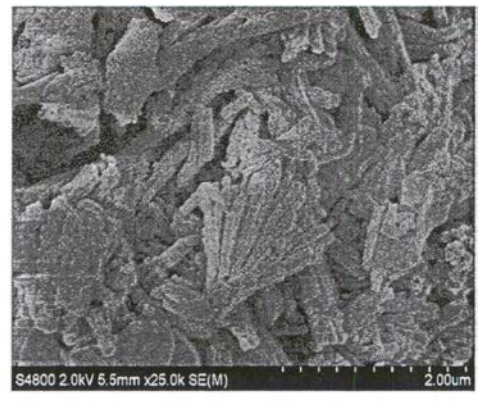

b)

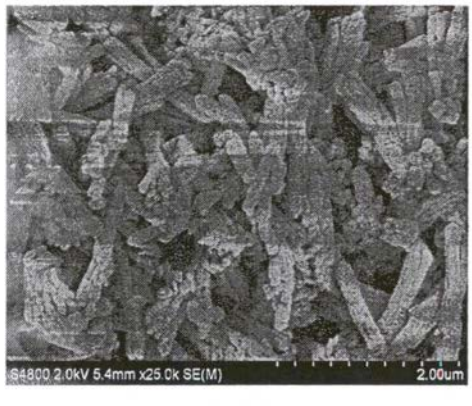

c)

d)

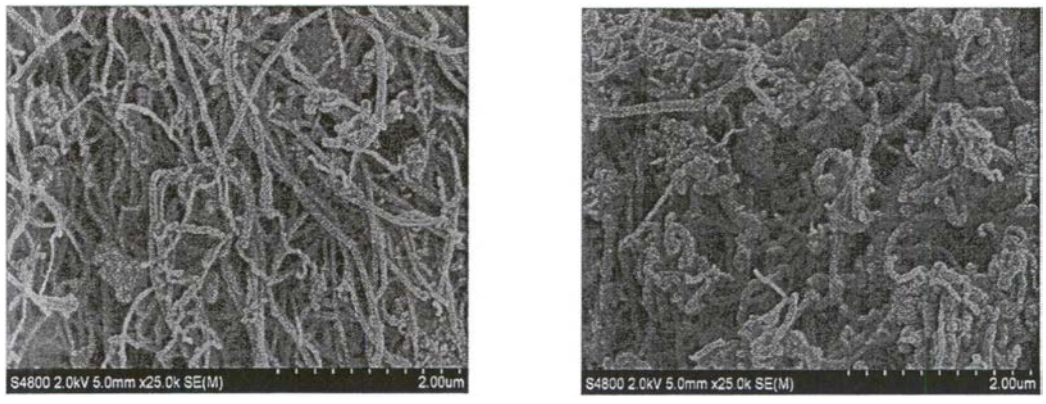

e) f)

Figure 4.30 SEM images of the spent catalysts a) CZO, b) CZM1O , c) CZM3O , d) 15Ni/CZO, e) 15Ni/CZM1O, f) 15Ni/CZM3O catalysts after exposure to MPO reaction (CH_4/O_2 = 2:1, GHSV = 53000 h^{-1}).